Mechanics of Materials 97 (2016) 48–58

Contents lists available at ScienceDirect

Mechanics of Materials

journal homepage: www.elsevier.com/locate/mechmat

Experimental observations on rate-dependent cyclic deformation of super-elastic NiTi shape memory alloy

Qianhua Kan[a], Chao Yu[b], Guozheng Kang[a,*], Jian Li[b], Wenyi Yan[c]

[a] State Key Laboratory of Traction Power, Southwest Jiaotong University, Chengdu, Sichuan 610031, PR. China
[b] Applied Mechanics and Structure Safety Key Laboratory of Sichuan Province, School of Mechanics and Engineering, Southwest Jiaotong University, Chengdu, Sichuan 610031, PR. China
[c] Department of Mechanical and Aerospace Engineering, Monash University, Clayton, VIC 3800, Australia

ARTICLE INFO

Article history:
Received 2 October 2015
Revised 17 February 2016
Available online 27 February 2016

Keywords:
NiTi shape memory alloy
Super-elasticity
Cyclic deformation
Rate-dependence
Internal heat production

ABSTRACT

Based on the strain-controlled cyclic tension-unloading tests at various strain rates (3.3×10^{-4}–3.3×10^{-2}/s), the effect of strain rate on the uniaxial cyclic deformation of a super-elastic NiTi shape memory alloy (SMA) was investigated. It is concluded that apparent degeneration of super-elasticity occurs during the cyclic loading, i.e., the residual strain and transformation hardening increase, but the start stress of forward transformation and the maximum responding stress decrease with the increasing number of cycles and strain rate, and finally reach to their saturated states after certain cycles. Although the dissipation energy per cycle decreases progressively during the cyclic loading and is saturated after certain cycles, it does not change monotonically with the increasing strain rate. Moreover, the temperature oscillation is observed due to the internal heat production from the inelastic dissipation and transformation latent heat, and the extent of temperature variation increases monotonically with the increasing strain rate, which is the physical nature of rate-dependent cyclic deformation of the NiTi SMA.

1. Introduction

Owing to its excellent dissipative performance and biological compatibility, super-elastic NiTi shape memory alloy (SMA) has been used in many fields, such as biomedicine, micro-electro-mechanical systems (MEMS), aerospace and civil engineering (Jani et al., 2014). In these applications, SMA components are often subjected to a cyclic loading involving a variation of loading rate. For example, in civil engineering, SMA-based components are often used as dampers in anti-seismic or cable structures (Helbert et al., 2014), where a rate-varied cyclic loading is applied. Therefore, it is required to understand the rate-dependent thermo-mechanical cyclic deformation of super-elastic NiTi SMAs, so that SMA smart devices are designed more efficiently.

In the last decades, experimental observations on the thermo-mechanical cyclic deformation of super-elastic NiTi SMAs were extensively conducted, which focused on two loading modes, i.e., strain- and stress-controlled ones. When the maximum strain is fixed, a residual strain occurs and accumulates in the cyclic tension-unloading tests, and the start stress of martensitic transformation and the dissipation energy per cycle decrease progressively; after certain cycles, a quasi-shakedown state is reached, as discussed by Miyazaki et al. (1986), Zhang et al. (2008), Nemat-Nasser et al. (2006), Strnadel et al. (1995a, 1995b), which represents the functional fatigue of super-elastic NiTi SMAs (Predki et al., 2006; Eggeler et al., 2004; Kang et al., 2012). Moreover, transformation ratcheting was observed under the stress-controlled cyclic loading

* Correspondent author. Tel.: +86 28 87603794; fax: +86 28 87600797.
E-mail address: guozhengkang@home.swjtu.edu.cn, guozhengkang@126.com (G. Kang).

http://dx.doi.org/10.1016/j.mechmat.2016.02.011
0167-6636/

conditions, which was dependent on the stress level (Kang et al., 2009, 2012) and loading path (Song et al., 2014).

It should be noted that the above-mentioned experimental observations on the cyclic deformation of super-elastic NiTi SMAs were performed at a specific loading rate; no rate-dependence of cyclic deformation was investigated. As discussed by Shaw and Kyriakides (1995), Grabe and Bruhns (2008), Yin et al. (2013), He and Sun (2010a), Kang and Kan (2010), Sun et al. (2012), obvious temperature variation occurs during the tension-unloading tests due to the internal heat production of NiTi SMAs, and its extent depends on the applied loading rate, which made the macroscopic transformation domains and transformation hardening increase with the increasing loading rate. Recently, rate-dependent cyclic deformation of super-elastic NiTi SMAs was investigated by some experimental observations (Nemat-Nasser et al., 2006; Morin et al., 2011; He and Sun, 2010b; Yin et al., 2014) and theoretical models (Zhu and Zhang, 2007; Morin et al., 2014; Yu et al., 2014a,b), and the effect of temperature variation on the martensitic transformation and its reverse was discussed. In these experiments, a trained NiTi SMA was used to exclude the effect of super-elasticity degeneration on the thermo-mechanical coupled cyclic deformation of the NiTi SMA. It was concluded that the macroscopic transformation domains and transformation hardening modulus increase with the increasing loading rate, but the stress–strain hysteresis loop does not vary with the loading rate monotonically; such rate-dependence is mainly caused by the competition between the internal heat production (coming from the mechanical dissipation and transformation latent heat) and heat exchange with the surroundings, which is different from that in ordinary metals caused by the viscosity (Kang et al., 2006). However, the interactions between super-elasticity degeneration and rate-dependence remain unrevealed yet for super-elastic NiTi SMAs.

Therefore, in this work, the uniaxial rate-dependent cyclic deformation of untrained super-elastic NiTi SMA is investigated by strain-controlled cyclic tension-unloading tests at room temperature. The effects of strain rate on the super-elasticity degeneration and temperature variation during the cyclic deformation are discussed. The cyclic stress–strain curves, evolutions of average temperature, and the temperature distribution along the axial direction of the specimen obtained at various strain rates are evaluated, respectively.

2. Experimental procedure

Polycrystalline super-elastic NiTi SMA micro-tubes (from Jiangyin Materials Development Co., Ltd., China) were used in the cyclic tension-unloading tests. The micro-tube was annealed at 500 °C for 30 min and cooled by oil quenching, but without experiencing any training. The nominal alloy composition determined by the X-ray diffraction spectroscopy was Ni, 50.32 at%. The finish and start temperatures of martensite and austenite phases M_f, M_s, A_f and A_s were measured to be –25.0, 9.7, –18.2 and 12.4 °C, respectively, by differential scanning calorimetry (DSC), as shown in Fig. 1. The initial phase of the alloy was

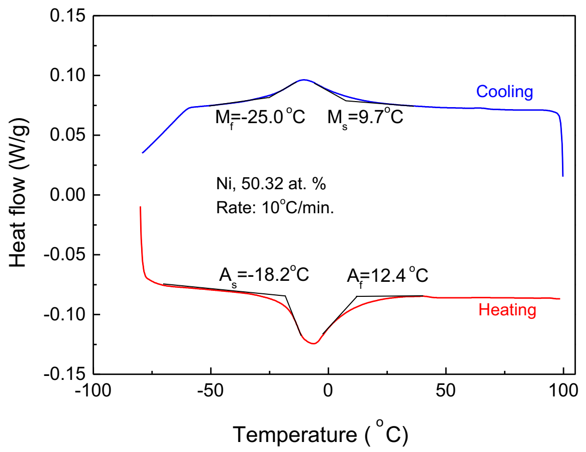

Fig. 1. Determination of zero-stress transformation temperature using a DSC.

austenite phase at room temperature (i.e., 26 °C), and the alloy exhibits super-elasticity.

All cyclic tests were performed under the strain-controlled conditions by the MTS858-BIONIX machine with a maximum load of 5 kN. Since a strong localization of martensite transformation in the super-elastic NiTi SMA, a heterogeneous strain field will exist along the axial direction of specimen and the measured strain by the extensometer should be denoted as a nominal strain. The tubular specimens with an outer diameter of 2.5 ± 0.02 mm and inner diameter of 2.2 ± 0.02 mm were cut from the as-received micro-tubes. The total length of the specimen is 60 mm and the gauge length of the extensometer is 15 mm. A pair of round plugs made by 42CrMo steel with a length of 15 mm and a diameter of 2.2 mm was inserted into the two ends of the micro-tube, and a pair of self-designed clamps with a continuous clamping pressure was used to grip the two ends of the micro-tube. Then, the new clamps were gripped by the clamps of MTS858-BIONIX machine.

Six nominal strain rates, i.e., 3.3×10^{-4}, 6.6×10^{-4}, 1×10^{-3}, 3.3×10^{-3}, 1×10^{-2} and 3.3×10^{-2}/s were prescribed in the cyclic tests. The maximum tensile strain for each load case was fixed as 9%. For the tests at lower strain rates (e.g., 3.3×10^{-4} and 6.6×10^{-4}/s), the number of cycles was prescribed to be 20; for the ones at higher strain rates (e.g., 1×10^{-3}, 3.3×10^{-3}, 1×10^{-2} and 3.3×10^{-2}/s), the number of cycles was prescribed to be 50. The test temperature is set to be 28 °C.

To investigate the thermal effect of the super-elastic NiTi SMA at different strain rates, a fast and sensitive infrared camera FLIR A655sc (from FLIR system AB Inc., Sweden) with a macro-focusing lens was placed near the tube to get simultaneous two-dimensional temperature map on the surface of the specimens. The FLIR A665sc has a high resolution of 640 × 480, which can cover the whole front surface of the micro-tube in each test. A temperature map can be selected by a rectangle box covering the gauge of the tube to evaluate the average temperature of all pixels by the FLIR ResearchIR. It is noted that the FLIR A665sc only captures the temperature field on the two-dimensional projection surface of the micro-tube; its

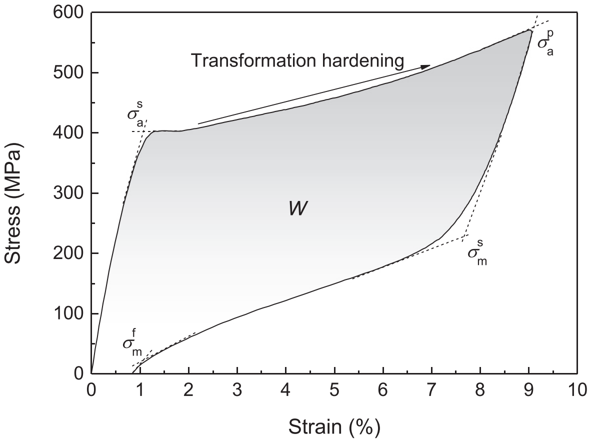

Fig. 2. Illustration of transformation stresses, transformation hardening and dissipation energy.

influence on the average temperature measurement under cyclic tension-unloading tests is neglected. It is stated that the mentioned temperatures in this work were obtained from the average temperature of all pixels located in the selected rectangle box.

Additional cyclic tests were also carried out to investigate the relation between the super-elasticity degeneration of NiTi SMAs and test temperature. The test temperature was controlled by the temperature-controlled chamber SDH4004 (from Chongqing Inborn instrument Co., LTD, China), the specimen was heated to a specific temperature by the temperature control box and kept 30 min to obtain a uniform temperature field. The temperature control error was limited within ± 0.5 °C. The test temperature varied from 20 to 100 °C and the strain rate was set as 3.3×10^{-3}/s.

3. Results

3.1. Super-elasticity degeneration at various strain rates

As shown in Fig. 2, σ_a^s, σ_a^p, $\sigma_m^s$and σ_m^f are the start stress of forward transformation, the peak stress of forward transformation, the start and final stresses of reverse transformation, respectively. The transformation hardening indicates the progressively increased driving force during forward transformation. The dissipation energy *W* represents the damping capability of NiTi SMA. It is an important indicator to evaluate the super-elasticity and can be calculated from the area surrounded by the stress–strain curve in each cycle.

Fig. 3 shows the cyclic stress–strain curves of the NiTi SMA micro-tubes obtained in the cyclic tension-unloading tests at various strain rates, i.e., 3.3×10^{-4}, 6.6×10^{-4}, 1×10^{-3}, 3.3×10^{-3}, 1×10^{-2} and 3.3×10^{-2}/s. The stress–strain curves obtained in the 1st, 2nd, 5th, 10th and 20th cycles are given for each loading case as shown in Fig. 3a–e, and the ones obtained in the 50th cycle are given in Fig. 3f for the loading cases at the higher strain rates (e.g., 1×10^{-3}, 3.3×10^{-3}, 1×10^{-2} and 3.3×10^{-2}/s). From Fig. 3a–e, it is seen that super-elasticity degeneration occurs at each strain rate, i.e., the residual strain accumulates during the cyclic tension-unloading, the start stress of forward transformation and the peak stress per cycle decrease, and the hysteresis loop becomes narrower and narrower with the increasing number of cycles; a saturated state is reached after certain cycles, which is similar to those observed in Strnadel et al (1995a, b), Eggeler et al (2004) and Kang et al. (2012).

Moreover, it is readily concluded from Fig. 4a that the evolutions of transformation stresses with the number of cycles depend strongly on the strain rate. The peak stress of forward transformation σ_a^p increases more rapidly with the increasing strain rate than the start stress of forward transformation σ_a^s in the 1st cycle (the maximum change in transformation stresses at different strain rates are 79 MPa and 16 MPa in 1st cycle for σ_a^p and σ_a^s, respectively, see Fig. 4b), which implies an increasing transformation hardening. In the subsequent cycles, the start stress of forward transformation σ_a^s begins to decrease rapidly, and the increment in the start stress of forward transformation σ_a^s is higher than that in the peak stresses of forward transformation σ_a^p since the increased internal stress can reduce the driving force of forward transformation (Yu et al., 2014a). It is worth noting that the finish stress of reverse transformation σ_m^f decreases with the increasing strain rate, but hardly changes with the increasing number of cycles at each strain rate.

It is seen from Fig. 5a that the residual strain accumulates with the increasing number of cycles and becomes more remarkable as the strain rate increases. When the strain rate is low (e.g., 3.3×10^{-4}/s), the residual strain is about 2.04% after 20 cycles; when the strain rate is high (e.g., 3.3×10^{-2}/s), it reaches 4.2%. However, the relationship between the residual strain and strain rate is strongly non-linear, as shown in Fig. 5b. For instance, only a small increment of residual strain (i.e., 0.15%) is observed in the 1st cycle when the strain rate increases from 3.3×10^{-4}/s to 1×10^{-3}/s; while, such increment is much larger (i.e., 0.94%) when the strain rate increases from 1×10^{-3}/s to 3.3×10^{-2}/s. It is concluded that the stress–strain responses of the NiTi SMA strongly depend on the number of cycles and strain rates, and important non-linear rules are observed in the evolutions of transformation stresses and residual strain.

The evolution curves of dissipation energy, which is defined as the area of stress–strain hysteresis loop per cycle, vs. the number of cycles and strain rate are shown in Fig. 6a and b, respectively. It is seen from Fig. 6a that the dissipation energy decreases rapidly with the increasing number of cycles in first five cycles at different strain rates and reaches to a quasi-shakedown state. From Fig. 6b, in the 1st cycle, it is seen that the maximum and minimum values of dissipation energy occur at the strain rates of 1×10^{-2}/s and 3.3×10^{-4}/s, respectively. However, after the 1st cycle, the two extreme points occur at the strain rates of 1×10^{-3}/s and 3.3×10^{-2}/s, respectively, which is different from those observed from a trained NiTi SMA (He and Sun, 2010; Yin et al., 2014; He and Sun, 2011).

3.2. Temperature variation

The temperature variation during the cyclic deformation of the super-elastic NiTi SMA depends on the

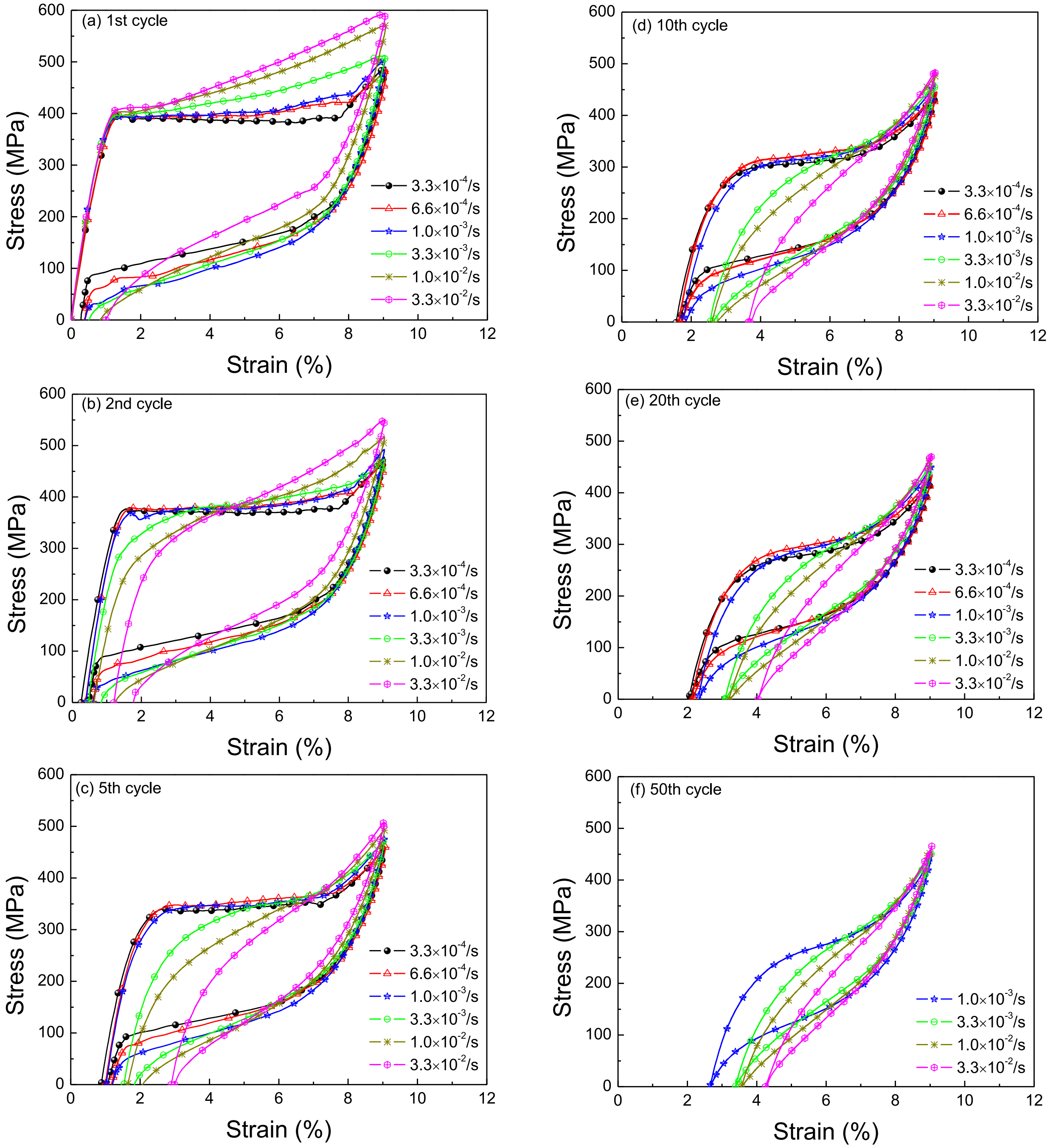

Fig. 3. Strain rate dependent cyclic stress–strain curves in different cycles: (a) 1st cycle; (a) 2nd cycle; (c) 5th cycle; (d) 10th cycle; (e) 20th cycle; (f) 50th cycle.

competition between the internal heat production and heat conduct, which is strongly dependent on the strain rate and is investigated in this subsection. Figs. 7 and 8 show the temperature variations recorded on the surface of the NiTi SMA micro-tube at two extreme strain rates, i.e., 3.3×10^{-4}/s and 3.3×10^{-2}/s, respectively. Eight critical points in the stress–strain curves are chosen at each strain rate, as shown in Figs. 7a and 8a. It is seen from Figs. 7b and 8b that the maximum and minimum temperatures at two strain rates during the 1st cycle are located at Points b (where the forward transformation finishes) and d (where the reverse transformation finishes), respectively. The distribution of temperature in the total measured region is initially non-homogeneous in the 1st cycle, but becomes

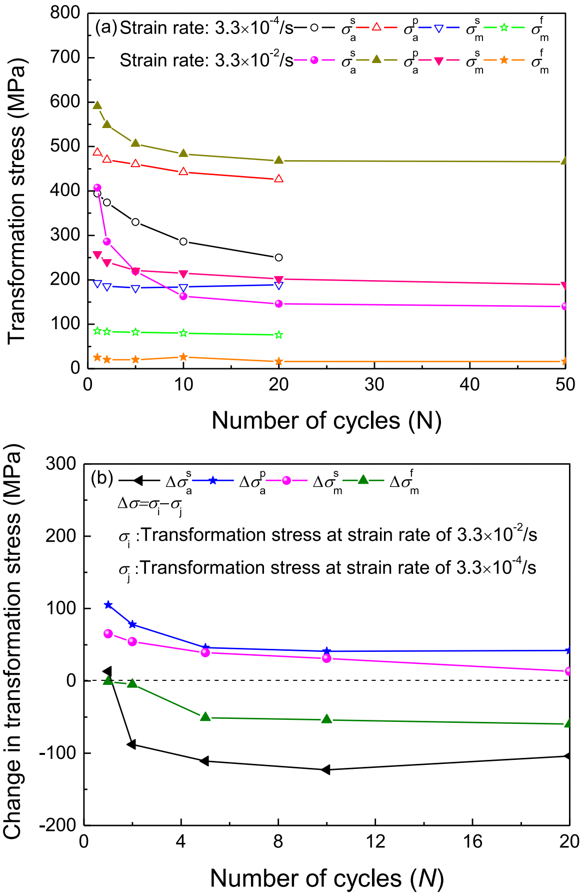

Fig. 4. Evolution curves of (a) transformation stress and (b) change in transformation stress vs. number of cycles.

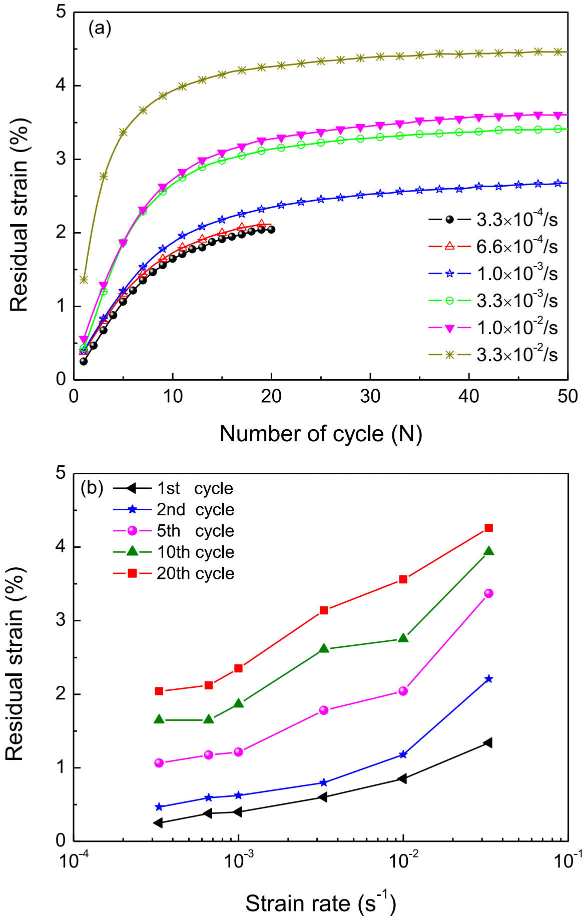

Fig. 5. Evolution curves of residual strain vs. (a) number of cycles and (b) strain rate.

relatively smooth in the 20th cycle. The temperature distributions along the axial direction of the specimen at two strain rates are given in Figs. 7c and 8c, respectively. It is seen that the temperature distribution is non-uniform in the 1st cycle due to the localized martensitic transformation, as commented in He and Sun (2010) and Sun et al. (2012). However, the heterogeneity of temperature distribution becomes weaker and weaker during the cyclic deformation due to the heat conduction within the specimen.

It is important to investigate the evolutions of temperature on the surface of specimen, which is corresponding to the evolutions of cyclic stress–strain curves shown in Fig. 3 (where, the nominal strain in the gauge length is used). The temperatures and their distributions obtained at various strain rates and in the 1st and 20th cycles are shown in Fig. 9a and b, respectively. The title “relative time” in *x* axis can be calculated by dividing the total time by the consumed time in each cycle, which is convenient for comparing the evolution of temperature in different time scales. It is seen from Fig. 9a that the temperature at each strain rate increases during the loading part per cycle due to the release of transformation latent heat in the forward transformation. During the unloading part per cycle, the temperature decreases at first since the latent heat is absorbed in the reverse transformation. When the reverse transformation is completed, the temperature is lower than the ambient temperature. During the following elastically unloading part, the temperature increases gradually due to the heat transfer with the ambient media. However, the temperature in the 20th cycles increases firstly and then decreases in the subsequent loading and unloading parts at all strain rates. Comparing Fig. 9a with b shows that the peak temperatures in the 1st cycle and at various strain rates occur at the end point of loading part; but in the 20th cycle, they are only observed before the end of loading part. It can be explained that a reduced maximum transformation strain results in a rapidly finished forward transformation before the end of loading part with the increasing strain rate in the 20th cycle, also see Fig. 3a and e, the transformation latent heat is released completely when the forward transformation finishes.

Fig. 10a to f shows the evolution curves of temperature vs. the number of cycles obtained at various strain rates, i.e., 3.3×10^{-4}, 1×10^{-3}, 3.3×10^{-3}, 1×10^{-2} and 3.3×10^{-2}/s, respectively. It is seen that an obvious temperature oscillation occurs due to the release/absorption of transformation latent heat (He and Sun, 2010; Yin et al., 2014). Moreover, at each strain rate, the amplitude of

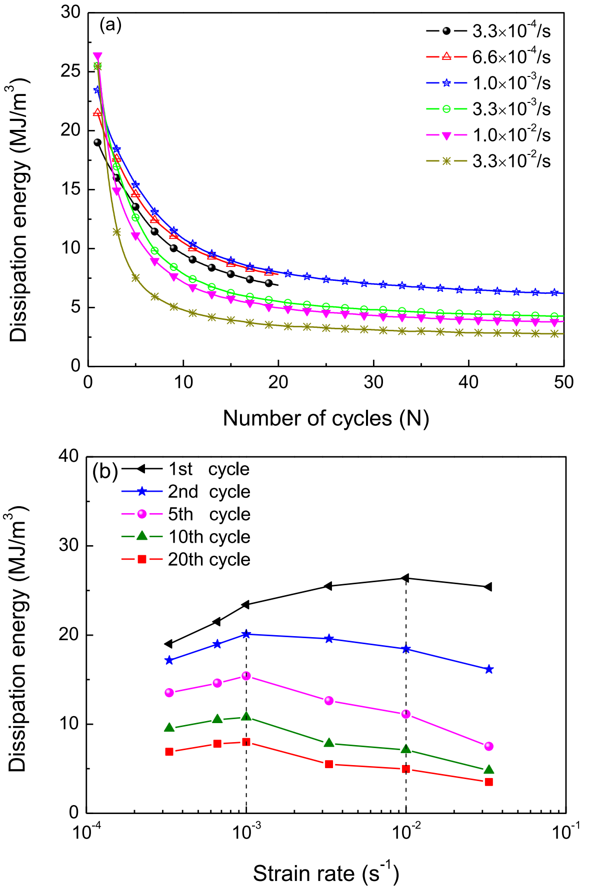

Fig. 6. Evolution of dissipation energy vs. (a) number of cycles and (b) strain rate.

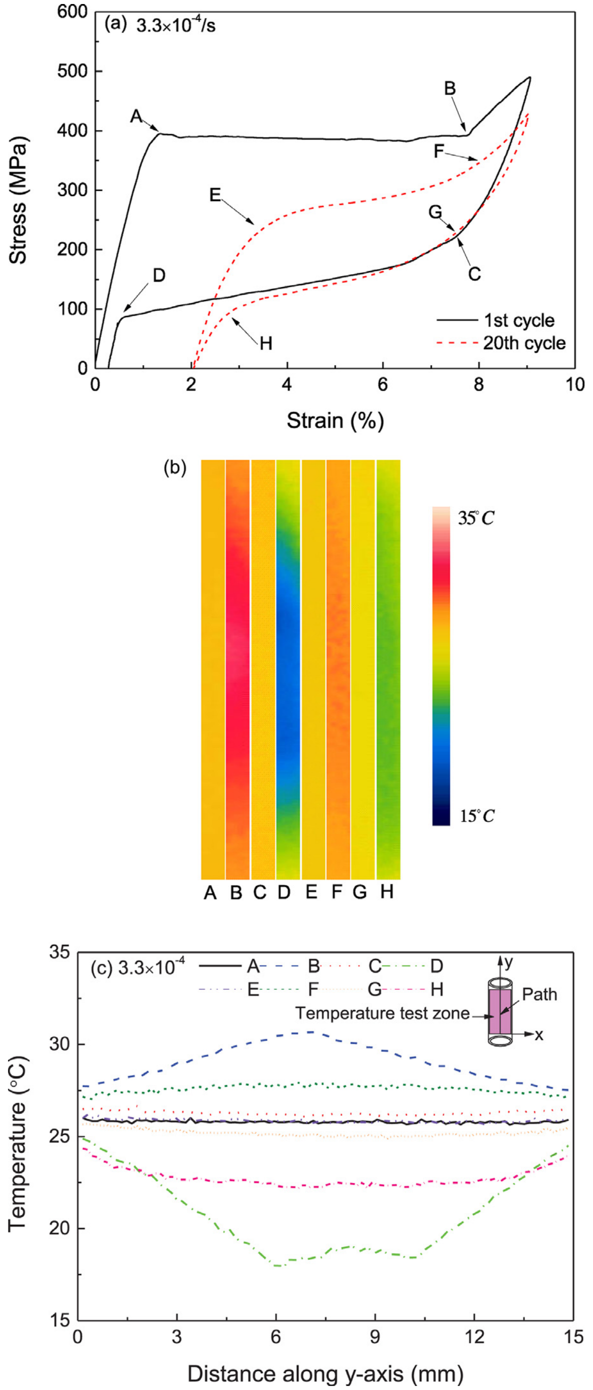

Fig. 7. Temperature field in the NiTi micro-tube at strain rate 3.3×10^{-4}/s: (a) specific observed points in the stress-strain curves; (b) temperature morphology at specific points; (c) temperature variation along the specific path at specific points.

temperature oscillation decreases with the increasing number of cycles. As discussed by Morin et al. (2011) and Yu et al. (2014b), the amount of transformation latent heat and intrinsic mechanical dissipation are directly proportional to the inelastic strain, including transformation strain and plastic strain. Owing to the accumulated residual strain caused by dislocation slipping, the maximum transformation strain produced in the martensitic transformation at each strain rate decreases with the increasing number of cycles, the amplitude of temperature oscillation decreases during the cyclic deformation.

Fig. 11a and b shows the evolution curves of the amplitudes and mean values of temperature oscillation vs. the number of cycles, respectively. From Fig. 11a, it is seen that the amplitude and mean values of temperature oscillation in a specific cycle varies non-monotonically with the increasing strain rate. The minimum amplitude and mean values of temperature oscillation in the stable cycle occur at the strain rate of 3.3×10^{-4}/s; however, the maximum amplitude and mean values of temperature oscillation in the stable cycle occur at the strain rates of 1×10^{-2}/s and 3.3×10^{-3}/s. Such non-monotonic variation can be explained by the two mechanisms: (1) when the strain rate is low, the heat transfer via convection and conduction is much faster than the heat production caused by the latent heat and inelastic dissipation. So, the temperature variation is not obvious and the amplitude of temperature oscillation is very small, as shown in Fig. 11a. When the strain rate is high, the heat production caused by the latent heat and inelastic dissipation is much faster

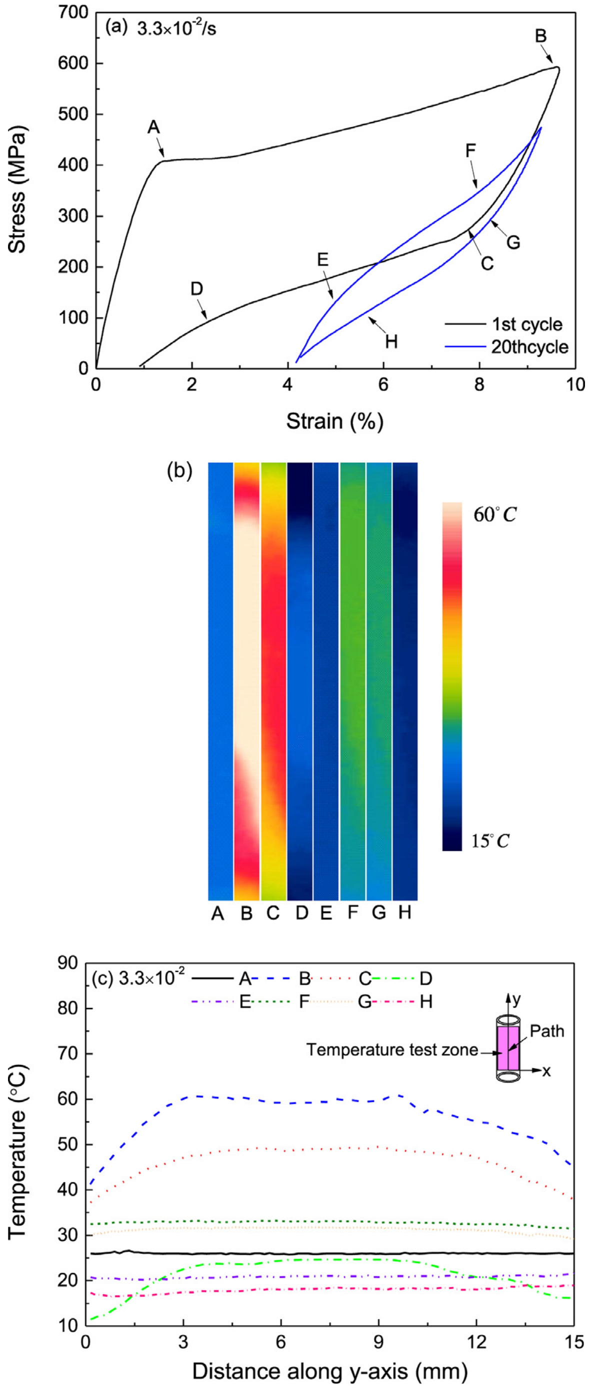

Fig. 8. Temperature field in the NiTi micro-tube at strain rate 3.3×10^{-2}/s: (a) specific observed points in the stress–strain curves; (b) temperature morphology at specific points; (c) temperature variation along the specific path at specific points.

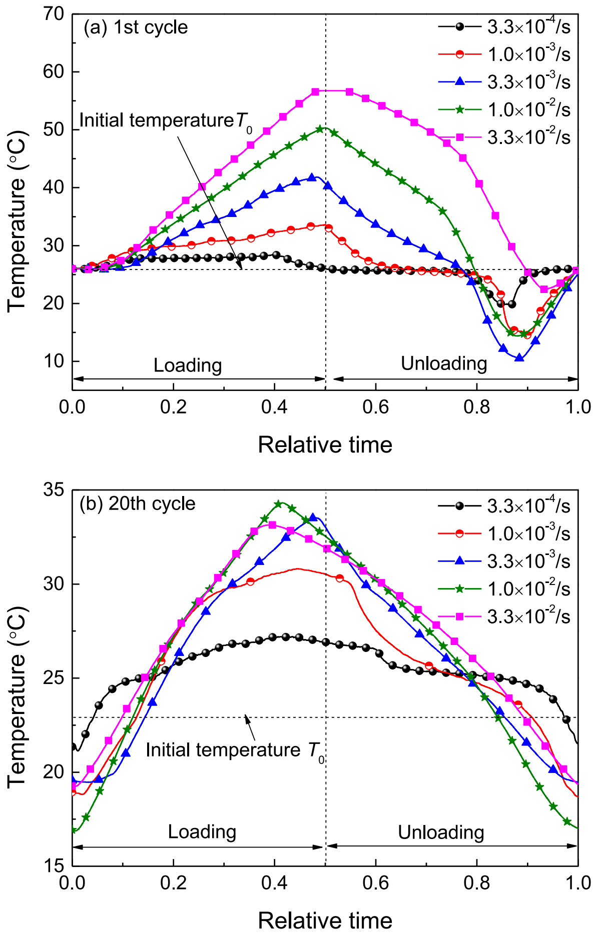

Fig. 9. Variation of temperatures at various strain rates: (a) in the 1st cycle; (b) in the 20th cycle.

than the heat transfer. Thus, the temperature variation becomes more and more remarkable and strong temperature oscillation is observed, as shown in Fig. 10e, and then the amplitude and mean values of temperature oscillation is relatively large, as shown in Fig. 11a and b. (2) As mentioned above, the residual strain in a given cycle increases with the increasing strain rate. Thus, the amount of the heat production in a given cycle caused by both latent heat and intrinsic mechanical dissipation decreases with the increasing strain rate since they are directly proportional to the martensitic transformation. These two competitive mechanisms lead to the non-monotonic variation in the amplitude and mean values of temperature oscillation.

4. Discussion

In Sections 3.1 and 3.2, the rate-dependent uniaxial cyclic deformation of super-elastic NiTi SMA is investigated. It is concluded that the evolution of the stress–strain curve strongly depends on the applied strain rate; more remarkable temperature variation occurs in the case at higher strain rate and the average temperature and its distribution change with the increasing number of cycles. Such findings imply that an interaction occurred among the stress, strain and temperature determines the rate-dependent cyclic deformation of super-elastic NiTi SMAs. In order to have a clear picture of such interaction, some discussions on the physical nature of rate-dependent cyclic

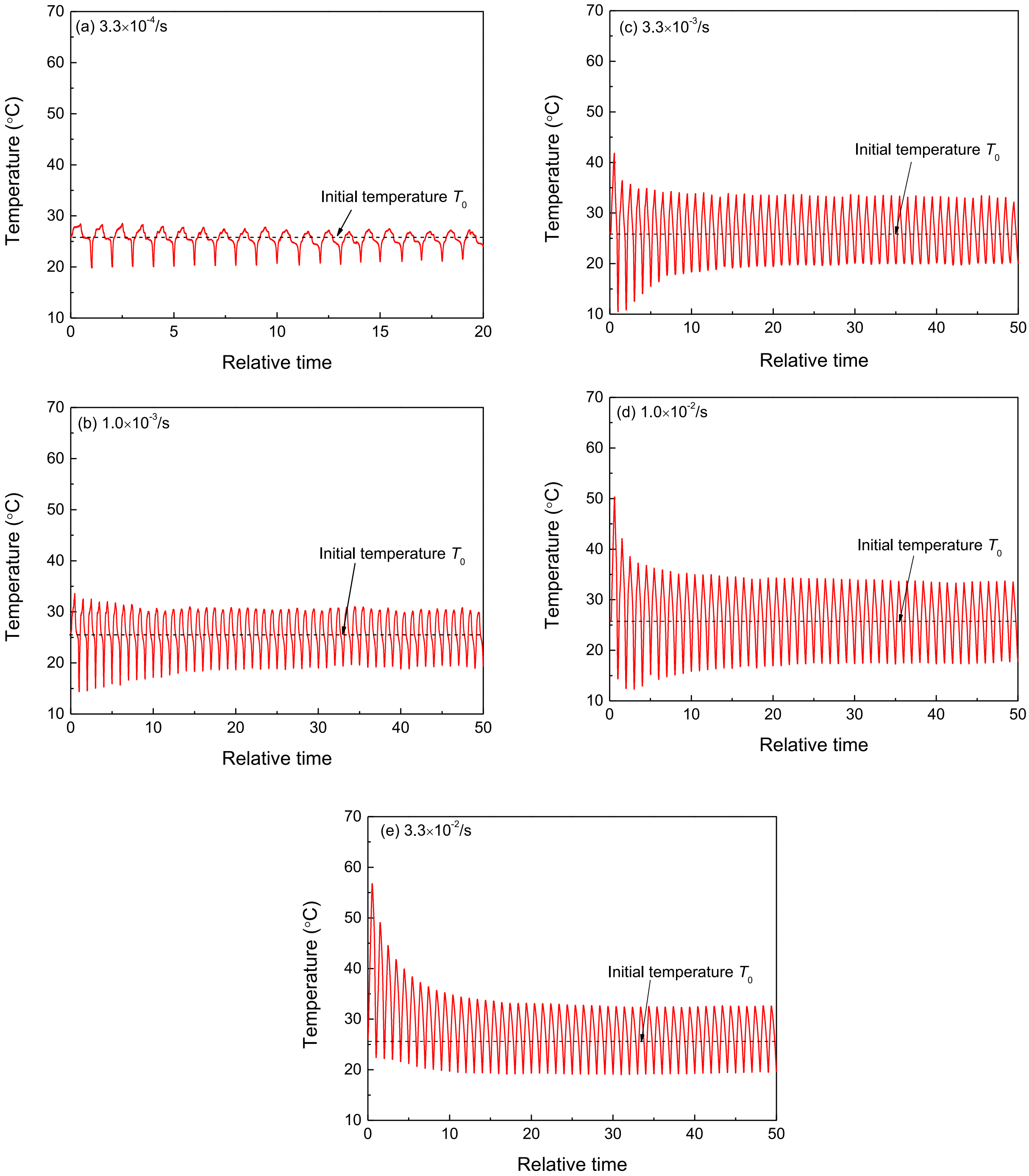

Fig. 10. Evolution curves of temperatures at various strain rates: (a) 3.3×10^{-4}/s; (b) 1×10^{-3}/s; (c) 3.3×10^{-3}/s; (d) 1×10^{-2}/s; (e) 3.3×10^{-2}/s.

deformation of super-elastic NiTi SMAs are presented in this subsection:

(1) Super-elasticity degeneration. From a physical standpoint, the super-elasticity degeneration of NiTi SMAs during a cyclic deformation can be attributed to the interaction between martensitic transformation and dislocation slipping. Different from the plastic deformation in ordinary metals, the dislocation slipping in super-elastic NiTi SMAs can be activated by the high local stress near the austenite-martensite interfaces during the repeated martensitic transformation and its reverse, even the overall applied stress is lower than the yield stress of austenite phase, as discussed by Hamilton et al. (2004), Norfleet et al. (2009) and Simon et al. (2010). With the help of

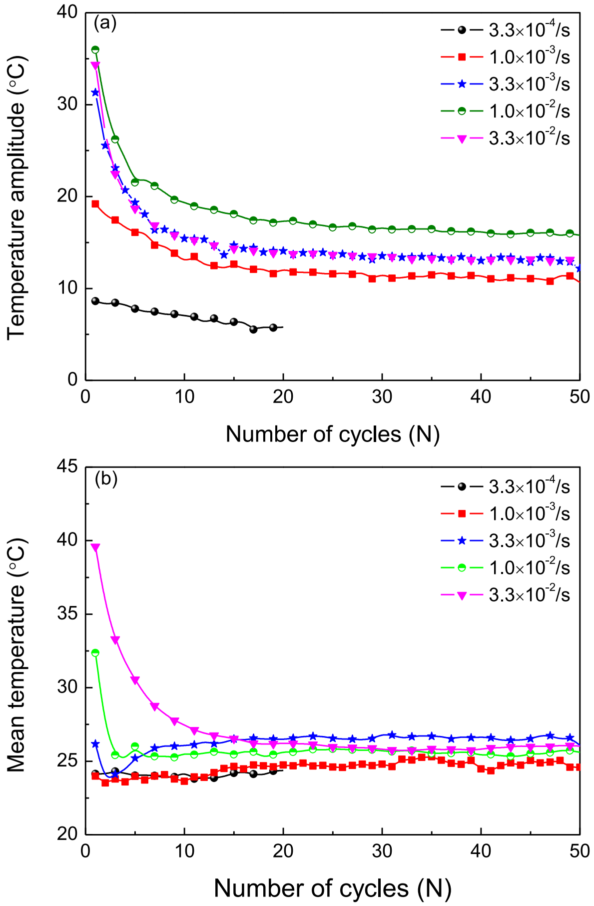

Fig. 11. Evolution curves of (a) temperature amplitude; (b) mean temperature vs. number of cycles at various strain rates.

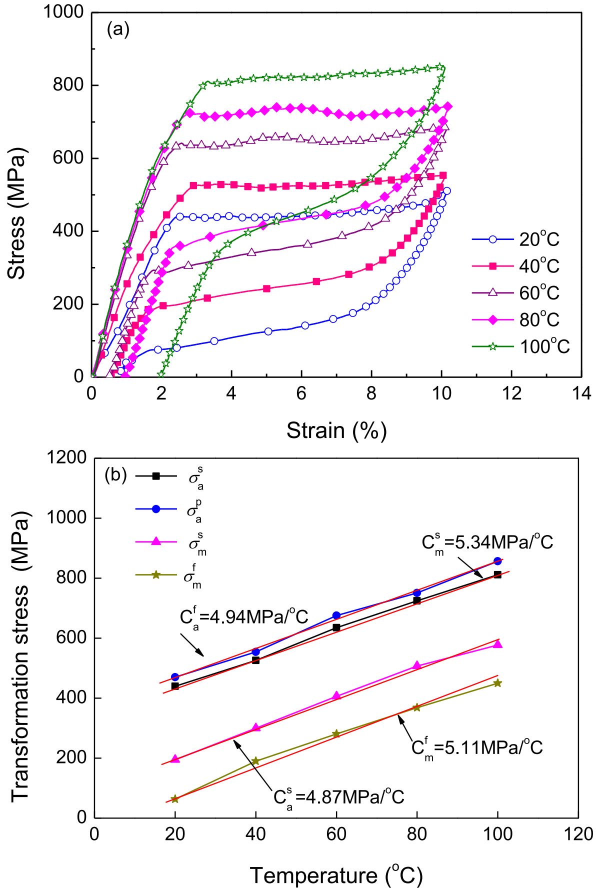

Fig. 12. Temperature-dependent transformation behaviours: (a) stress–strain curves; (b) curves of transformation stress vs. temperature.

such local stress caused by the unmatched inelasticity of austenite and martensite phases, the total stress in the austenite matrix close to the transformation front can exceed the yield stress of austenite phase. In the meantime, as observed by Delville et al. (2010); Delville et al. (2011), Pelton et al. (2012) and Brinson et al. (2004), the dislocation density of NiTi SMAs increases rapidly during the cyclic deformation. An internal stress can be induced by an increasing dislocation density, and can assist the nucleation of stress-induced martensite (Miyazaki et al., 1986). Since the stress field in the alloy is disturbed by the internal stress, a stress gradient occurs and then hinders the growth of martensite variants (Yawny et al., 2005). Thus, it is seen from the macroscopic stress–strain curves that the start stress of martensitic transformation decreases but the transformation hardening modulus increases with the increasing number of cycles during the cyclic deformation. Moreover, some of the induced martensite variants can be pinned by the dislocations and the reverse transformation cannot be completed thoroughly. Thus, residual martensite phase can be observed after progressive cycles.

(2) Temperature-dependent cyclic deformation behaviour: Besides the Clausius–Claperyon relation between transformation stress and temperature, the super-elasticity degeneration of NiTi SMAs depends strongly on the test temperature, and the stress–strain curves rise with an increased test temperature, as validated in Fig. 12a. On the one hand, the four critical stresses of martensitic transformation (start and finish stresses of forward transformation and the corresponding ones of reverse transformation) almost increase linearly with the increasing test temperature (see Fig. 12b), leading to the increasing driving force of dislocation slipping. Thus, it is observed that the residual strain increases with the increasing test temperature (Yu et al., 2014a). It is noted that the residual strain can be influenced by the test temperature and strain rate simultaneously, but the increased test temperature can provide more remarkable residual strain than the increased strain rate by comparing Fig. 3a and Fig. 12a. It is the reason why the temperature caused by the transformation latent and intrinsic dissipation keeps oscillating in each cycle (see Fig. 9a); the maximum of the increased temperature is only 28.8 °C. However, the test temperature in

Fig. 12a increases from 20 °C to 100 °C but it keeps a constant value in one cycle. At a higher test temperature, owing to the higher dislocation density, the internal stress induced by the dislocation and the stress gradient are much larger than those at a lower test temperature. Thus, the super-elasticity degeneration during cyclic deformation becomes more and more obvious with the increasing test temperature.

(3) Thermo-mechanical coupling effect: the internal heat production coming from the mechanical dissipation and transformation latent heat competes against the heat transfer/convection during inelastic deformation, which leads to the variation in the amplitude and mean values of temperature oscillation in the specimen. In the meantime, the temperature variation can affect the cyclic deformation of NiTi SMAs since the super-elasticity degeneration depends strongly on the temperature. Therefore, the rate-dependence of cyclic deformation is a result of temperature effect in nature; the temperature variation depends on the loading rate, i.e., a competition between the internal heat production and external heat exchange.

The above-mentioned three factors leading to the super-elasticity degeneration of NiTi SMAs during the cyclic deformation depends strongly on the loading rate. Surely, these discussions will contribute to constructing a physical mechanism-based constitutive model considering thermo-mechanical coupling in order to predict the rate-dependent super-elasticity degeneration of untrained NiTi SMAs during the cyclic deformation in further work.

5. Conclusions

In this work, the rate-dependent cyclic deformation of super-elastic NiTi SMA was investigated by strain-controlled cyclic tension-unloading tests at various strain rates ranging from 3.3×10^{-4}/s to 3.3×10^{-2}/s. The following conclusions are drawn out:

(1) The residual strain and transformation hardening increase with the increasing number of cycles and strain rates, but the dissipation energy decreases with the increasing number of cycles, and increases firstly and then decreases with the increasing strain rate.

(2) Temperature oscillation occurs at each strain rate. During the cyclic deformation, the oscillation amplitude decreases with the increasing number of cycles and tends to be saturated after certain cycles.

(3) Super-elasticity degeneration and the evolutions of temperature exhibit strong rate-dependence. The residual strain and transformation hardening increase, but the start stress of transformation and peak stress decrease with the increasing strain rate. However, the dissipation energy, the amplitude and mean values of temperature oscillation non-monotonically change with the increasing strain rate.

(4) The rate-dependent cyclic deformation of NiTi SMA is attributed to three main mechanisms, i.e., super-elasticity degeneration, temperature-dependence and thermo-mechanical coupling effect.

Acknowledgments

Financial supports by the National Natural Science Foundation of China (11202171; 11572265; 11532010), the project for Sichuan Provincial Youth Science and Technology Innovation Team and China (2013TD0004) and the open project of State Key Laboratory for Strength and Vibration of Mechanical Structures (SV2014-KF-11) are acknowledged.

References

Brinson, L.C., Schmidt, I., Lammering, R., 2004. Stress-induced transformation behavior of a polycrystalline NiTi shape memory alloy: micro and macromechanical investigations via in situ optical microscopy. J. Mech. Phys. Solids 52, 1549–1571.

Delville, R., Malard, B., Pilch, J., Sittner, P., Schryvers, D., 2010. Microstructure changes during non-conventional heat treatment of thin Ni-Ti wires by pulsed electric current studied by transmission electron microscopy. Acta Mater. 58, 4503–4515.

Delville, R., Malard, B., Pilch, J., Sittner, P., Schryvers, D., 2011. Transmission electron microscopy investigation of dislocation slip during superelastic cycling of Ni-Ti wires. Int. J. Plast. 27, 282–297.

Eggeler, G., Hornbogen, E., Yawny, A., Heckmann, A., Wagner, M., 2004. Structural and functional fatigue of NiTi shape memory alloys. Mater. Sci. Eng. A 378, 24–33.

Grabe, C., Bruhns, O.T., 2008. On the viscous and strain rate dependent behavior of polycrystalline NiTi. Int. J. Solids Struct. 45, 1876–1895.

Hamilton, R.F., Sehitoglu, H., Chumlyakov, Y., Maier, H.J., 2004. Stress dependence of the hysteresis in single crystal NiTi alloys. Acta Mater. 52, 3383–3402.

He, Y.J., Sun, Q.P., 2010a. Frequency-dependent temperature evolution in NiTi shape memory alloy under cyclic loading. Smart Mater. Struct. 19, 115014.

He, Y.J., Sun, Q.P., 2010b. Rate-dependence domain spacing in a stretched NiTi strip. Int. J. Solids Struct. 47, 2775–2783.

He, Y.J., Sun, Q.P., 2011. On non-monotonic rate dependence of stress hysteresis of superelastic shape memory alloy bars. Int. J. Solids Struct. 48, 1688–1695.

Helbert, G., Saint-Sulpice, L., Chirani, S.A., Dieng, L., Lecompte, T., Calloch, S., Pilvin, P., 2014. Experimental characterisation of three-phase NiTi wires under tension. Mech. Mater. 79, 85–101.

Jani, J.M., Leary, M., Subic, A., Gibson, M.A., 2014. A review of shape memory alloy research, applications and opportunities. Mater. Des. 56, 1078–1113.

Kan, Q.H., Kang, G.Z., 2010. Constitutive model for uniaxial transformation ratchetting of super-elastic NiTi shape memory alloy at room temperature. Int. J. Plast. 26, 441–465.

Kang, G.Z., Kan, Q.H., Qian, L.M., Liu, Y.J., 2009. Ratchetting deformation of super-elastic and shape-memory NiTi alloys. Mech. Mater. 41, 139–153.

Kang, G.Z., Kan, Q.H., Yu, C., Song, D., Liu, Y.J., 2012. Whole-life transformation ratchetting and fatigue of super-elastic NiTi Alloy under uniaxial stress-controlled cyclic loading. Mater. Sci. Eng. A 535, 228–234.

Kang, G.Z., Kan, Q.H., Zhang, J., Sun, Y.F., 2006. Time-dependent ratcheting experiments of SS304 stainless steel. Int. J. Plast. 22, 858–894.

Miyazaki, S., Imai, T., Igo, Y., Otsuka, K., 1986. Effect of cyclic deformation on the pseudoelasticity characteristics of Ti-Ni alloys. Metall. Mater. Trans. A 117, 115–120.

Morin, C., Moumni, Z., Zaki, W., 2011. Thermomechanical coupling in shape memory alloys under cyclic loadings: Experimental analysis and constitutive modeling. Int. J. Plast. 27, 1959–1980.

Morin, C., Moumni, Z., Zaki, W., 2014. A constitutive model for shape memory alloys accounting for thermomechanical coupling. Int. J. Plast. 27, 748–767.

Nemat-Nasser, S., Guo, W.G., 2006. Superelastic and cyclic response of NiTi SMA at various strain rates and temperatures. Mech. Mater. 38, 463–474.

Norfleet, D.M., Sarosi, P.M., Manchiraju, S., Wagner, M.X., Uchic, M.D., Anderson, P.M., Mills, M.J., 2009. Transformation-induced plasticity during pseudoelastic deformation in Ni-Ti microcrystals. Acta Mater. 57, 3549–3561.

Pelton, A.R., Huang, G.H., Moine, P., Sinclair, R., 2012. Effects of thermal cycling on microstructure and properties in Nitinol. Mater. Sci. Eng. A 532, 130–138.

Predki, W., Kloenne, M., Knopik, A., 2006. Cyclic torsional loading of pseudoelastic NiTi shape memory alloys: damping and fatigue failure. Mater. Sci. Eng. A 417, 182–189.

Shaw, J.A., Kyriakides, S., 1995. Thermomechanical aspects of NiTi. J. Mech. Phys. Solids 43, 1243–1281.

Simon, T., Kröger, A., Somsen, C., Dlouhy, A., Eggeler, G., 2010. On the multiplication of dislocations during martensitic transformations in NiTi shape memory alloys. Acta Mater. 58, 1850–1860.

Song, D., Kang, G.Z., Kan, Q.H., Yu, C., Zhang, C., 2014. Non-proportional multiaxial transformation ratchetting of super-elastic NiTi shape memory alloy: Experimental observations. Mech. Mater. 70, 94–105.

Strnadel, B., Ohashi, S., Ohtsuka, H., Miyazaki, S., Ishihara, T., 1995a. Effect of mechanical cycling on the pseudoelasticity characteristics of Ti-Ni and Ti-Ni-Cu alloys. Mater. Sci. Eng. A 203, 187–196.

Strnadel, B., Ohashi, S., Ohtsuka, H., Ishihara, T., Miyazaki, S., 1995b. Cyclic stress-strain characteristics of Ti-Ni and Ti-Ni-Cu shape memory alloys. Mater. Sci. Eng. A 202, 148–156.

Sun, Q.P., Zhao, H., Zhou, R., Saletti, D., Yin, H., 2012. Recent advances in spatiotemporal evolution of thermomechanical fields during the solid-solid phase transition. Compt. Rend. Mecanique 340, 349–358.

Yawny, A., Sade, M., Eggeler, G., 2005. Pseudoelastic cycling of ultra-fine-grained NiTi shape-memory wires. Z. Metallkd. 96, 608–618.

Yin, H., Yan, Y., Huo, Y.Z., Sun, Q.P., 2013. Rate dependent damping of single crystal CuAlNi shape memory alloy. Mater. Lett. 109, 287–290.

Yin, H., He, Y.J., Sun, Q.P., 2014. Effect of deformation frequency on temperature and stress oscillations in cyclic phase transition of NiTi shape memory alloy. J. Mech. Phys. Solids 67, 100–128.

Yu, C., Kang, G.Z., Kan, Q.H., 2014a. A physical mechanism based constitutive model for temperature-dependent transformation ratchetting of NiTi shape memory alloy: One-dimensional model. Mech. Mater. 78, 1–10.

Yu, C., Kang, G.Z., Kan, Q.H., 2014b. Study on the rate-dependent cyclic deformation of super-elastic NiTi shape memory alloy based on a new crystal plasticity constitutive model. Int. J. Solids Struct. 51, 4386–4405.

Zhang, X.P., Liu, H.Y., Yuan, B., Zhang, Y.P., 2008. Superelasticity decay of porous NiTi shape memory alloys under cyclic strain-controlled fatigue conditions. Mater. Sci. Eng. A 481-482, 170–173.

Zhu, S.Y., Zhang, Y.F., 2007. A thermomechanical constitutive model for superelastic SMA wire with strain-rate dependence. Smart Mater. Struct. 16, 1696–1707.